Available online at www.sciencedirect.com
ScienceDirect
Journal of Molecular Catalysis A: Chemical 272 (2007) 75–83
JOURNAL OF MOLECULAR CATALYSIS A: CHEMICAL
www.elsevier.com/locate/molcata

One-step synthesis of methyl isobutyl ketone from acetone over Pd/MCM-22 zeolites

Piaoping Yang [a,*], Yongchen Shang [b], Jianfeng Yu [c], Jun Wang [a], Milin Zhang [a], Tonghao Wu [c]

[a] *College of Material Science and Chemical Engineering, Harbin Engineering University, Harbin 150001, PR China*
[b] *College of Chemistry, Harbin Normal University, Harbin 150023, PR China*
[c] *College of Chemistry, Jilin University, Changchun 130021, PR China*

Received 30 December 2006; received in revised form 14 March 2007; accepted 15 March 2007
Available online 20 March 2007

Abstract

MCM-22 zeolites with different Si/Al ratios were dynamically synthesized through hydrothermal method, and the Pd/MCM-22 catalysts were prepared by ion-exchange method as well. The physicochemical properties of the samples were well characterized by XRD, SEM, TEM, N_2 adsorption, NH_3-TPD, and FT-IR of d_3-acetonitrile adsorption. MCM-22 synthesized was markedly different from those in previous literatures, showing much smaller crystals. MCM-22 with Si/Al ratio of 25 showed the highest crystallinity and concentration of Brønsted acid sites. The loading of Pd particles had little influence on the structural and porous properties of MCM-22 zeolite. The specific surface area, pore volume, pore diameter, and the concentrations of the acid sites all decreased with increasing Pd loading as expected. One-step synthesis of methyl isobutyl ketone from acetone was investigated over Pd/MCM-22 catalysts. An acetone conversion of 34.0% and a selectivity of 86.9% for MIBK were realized. The catalytic results also suggested that a proper balance between metallic and acidic sites was necessary for obtaining high catalytic performance.
© 2007 Elsevier B.V. All rights reserved.

Keywords: MCM-22; Acetone; Methyl isobutyl ketone; One-step synthesis

1. Introduction

MCM-22 zeolite which presents a novel porous structure was first synthesized by Mobil in 1990 [1]. This peculiar structure of this zeolite consists of two independent pore systems both accessible through 10-membered ring (MR) apertures (4.0 × 5.5 Å) [2]. One pore system is composed of 12 MR large supercages with an inner diameter of 7.1 Å and a height of 18.2 Å, which are connected to one another through 10 MR windows. The second pore system is a two-dimensional sinusoidal channels system. MCM-22 zeolite, which presents unique porous structure, has showed its potential applications in many catalytic reactions, such as alkylation [3,4], isomerization [5,6], and cracking [7,8].

Methyl isobutyl ketone (MIBK) has been widely used in the fields of solvent and protective coating as one of the most important chemical products derived from acetone. The conventional process for MIBK synthesis consists of the following three steps: (i) aldol condensation of acetone to diacetone alcohol (DAA) over acid catalysts; (ii) acid-catalyzed DAA dehydration to mesityl oxide (MO); and (iii) selective hydrogenation of MO to MIBK over metal supported catalysts [9]. The first two steps are usually limited by the equilibrium, and the third process may produce a lot of side-products, which greatly reduce the selectivity for MIBK. Furthermore, a corrosive problem may also exist in the process due to the used liquid acid catalysts. Therefore, these drawbacks strongly stimulate the research on one-step synthesis of MIBK using a catalyst with condensation, dehydration and hydrogenation functions. These multiple-functional catalysts can act by shifting the equilibrium in the condensation step in favor of MO by simultaneous and irreversible hydrogenation it to MIBK. In the past two decades, many works have been reported on one-step synthesis of MIBK from acetone over metal supported catalysts, such as Pd/resin [10], Pd/hydrotalcites [11], Ni/MgO [12], Pd/Niobic acid [13], Pd/HMFI [14], Cu/MgO [15], Ni/ALPON [16], Na/Pd/MgO

* Corresponding author. Tel.: +86 431 85262614.
E-mail address: piaoping@ciac.jl.cn (P. Yang).

1381-1169/$ – see front matter © 2007 Elsevier B.V. All rights reserved.
doi:10.1016/j.molcata.2007.03.037

[17], Pt/HZSM-5 [18], Ni/Al_2O_3 [19], Pd/MCM-56 [20], and Pd/(Nb_2O_5/SiO_2) [21].

In this paper, we described the hydrothermal synthesis of MCM-22 zeolites with different Si/Al ratios. XRD, TEM, NH_3-TPD, and FT-IR techniques were used to examine the influence of Si/Al molar ratio on the structural, morphological, porous, and acidic properties of MCM-22 zeolites. In addition, the catalytic performance of Pd/MCM-22 catalysts was examined in one-step synthesis of MIBK from acetone. The influence of reaction conditions on the catalytic activity and stability test was also studied as well.

2. Experimental

2.1. Synthesis of materials

MCM-22 zeolite was synthesized according to the literature [22] using hexamethyleneimine (HMI) as organic template. The zeolite was obtained with the following molar compositions. SiO_2:Al_2O_3:NaOH:HMI:H_2O = 1:0.02:0.07:0.35:18.9. In a typical process, 2.282 g of $NaAlO_2$ and 20 mL of HMI were first added to a solution of 0.2 g NaOH diluted in 80 mL of H_2O and stirred until dissolved. Then, 120 g of silica was slowly added to the solution with vigorous stirring and maintained for 2 h. After this, the slurry was introduced into a 40 mL stainless steel autoclave, and dynamically crystallized at 443 K for 3 days with a rotation speed of 45 rpm/min. After the synthesis, the as-synthesized NaMCM-22 sample was thoroughly washed with distilled water, dried at 393 K for 12 h and then calcined at 823 K for 12 h. HMCM-22 was prepared by ion-exchange of NaMCM-22 with 1 M NH_4NO_3 solution at room temperature for 30 h for three times. The resulting HMCM-22 zeolite with Si/Al ratio of 25 was designed as MCM-22. HMCM-22 zeolites with Si/Al ratios of 15, 35, and 45 were synthesized by the same process, which were designed as MCM-22-15, MCM-22-35, and MCM-22-45, respectively. The corresponding Pd/MCM-22 catalysts were prepared by the ion-exchange method, using aqueous solution of palladium nitrate. Ion-exchange was carried out on a rotator–evaporator system for 48 h at 353 K. The prepared Pd/MCM-22 catalysts were dried at 353 K for 5 h and calcined at 823 K for another 5 h. The resulting catalysts were designated as *x*Pd/MCM-22 (*x* refers to the amount of stoichiometric Pd loading).

2.2. Characterization

X-ray diffraction (XRD) patterns were performed on a Shimadzu XRD–6000 diffractometer operating at 40 kV and 30 mA, using Cu Kα radiation (λ = 0.1542 nm). Scanning electron microscope (SEM) was inspected on a FEI XL30 ESEM FEG and transmission electron microscope (TEM) was performed on a FEI Tecnai G2 S-Twin electron microscope operating at 200 kV. N_2 adsorption was performed on a Micromeritics 2020 M apparatus. Pore size distribution was calculated from the adsorption branch of N_2 adsorption/desorption isotherm. The specific surface areas were determined using the BET method, and the pore volume was obtained by t-plot method.

NH_3-TPD which was used to examine the acidity of the catalysts was performed on a self-designed apparatus. Typically, a sample of 50 mg was first pretreated in argon at 873 K for 40 min, then cooled to 373 K and saturated at this temperature with ammonia until equilibrium. The NH_3-TPD profiles were recorded via a thermal conductivity detector with a heating rate of 10 K/min from 373 to 923 K in a helium flow.

The concentration of Brønsted and Lewis acid sites of the samples was determined by FT-IR spectroscopy after the adsorption of d_3-acetonitrile, performing on a Nicolet Impact–410 spectrometer. In comparison with pyridine, d_3-acetonitrile is a smaller and more sensitive probe molecule which was used to detect the presence of both Brønsted and Lewis sites in the zeolites channels [23,24]. Prior to the measurement, the samples were pressed in the form of self-supported wafers (thickness equivalent to 4–6 mg/cm^2), fixed in a quartz holder and then introduced into an infrared cell with NaCl windows. d_3-Acetonitrile was pretreated by freeze–pump–thaw cycles. Before the adsorption of d_3-acetonitrile, the samples were treated in situ by evacuation at 623 K in 10^{-3} Pa. Adsorption was then carried out at 298 K for 20 min, followed by an evacuation at the same temperature. For a quantitative characterization of the Brønsted acid sites (B), the C≡N–B vibration at 2296 cm^{-1} was used with an extinction coefficient of $\varepsilon(B) = 2.05 \pm 0.1$ cm μmol^{-1}. And for a quantitative evaluation of the Lewis acid sites (L), the C≡N–L vibration at 2323 cm^{-1} was used with the extinction coefficient of $\varepsilon(L) = 3.6 \pm 0.2$ cm μmol^{-1} [23].

The exact Pd loading of the catalysts was determined by ICP-PLASMA 1000 after the digestion of the sample with HF solution. The metal Pd dispersion and the metal particle size were determined by H_2-TPD method on a self-designed apparatus. In a typical process, the catalyst (100 mg) was first reduced by H_2 from room temperature to 673 K at 10 K/min and kept for 2 h. After this, the sample was flushed with argon, then cooled to room temperature in H_2 flow and stayed for 1 h to reach adsorption/desorption equilibrium. Subsequently, the adsorbed hydrogen was desorbed from room temperature to 873 K at 10 K/min and monitored via a thermal-conductivity detector. The metal dispersion was measured from the amount of adsorbed H_2 (mmol/g), the metal loading (mmol metal/g), and the adsorption stoichiometry. The dissociative chemisorption of H_2 on Pd (1 H_2 molecule adsorbing on 2 Pd sites, $2Pd + H_2 \rightarrow 2Pd\text{-}H$) was used for the H_2-based dispersion measurements [25,26].

2.3. Catalytic test

The catalytic tests were carried out on a fixed bed tubular reactor using 0.5 g catalyst at high pressure. Before reaction, the catalysts were reduced "in situ" in flowing hydrogen at 673 K for 3 h and then cooled down to the reaction temperature. The stream of gas mixture of hydrogen and acetone was introduced at a constant rate into the upper zone of the reactor, where SiO_2 pellets were packed for maintaining the reaction temperature for preheating and vaporization. The reaction products were analyzed by on-line gas chromatography (Shimadzu GC–14B)

equipped with a Shimadzu fused silica capillary column (code: CBP–M50–025).

3. Results and discussion

3.1. Characterization of the MCM-22 zeolites with different Si/Al molar ratio

Fig. 1 depicts the XRD patterns of MCM-22 with different Si/Al molar ratios. As shown in the figure, no obvious diffractions can be found between 1° and 5° of 2θ degree (Fig. 1A), demonstrating the poor order of the porous structure for the samples. While in the XRD patterns between 5° and 45° (Fig. 1B), the diffractions of the typical MWW structure are sharp and obvious. The positions and intensities are well consistent with those reported by the literature [22], suggesting the high purity and good crystallinity of HMCM-22 zeolites with different Si/Al ratios. It can be also found that HMCM-22 with Si/Al = 25 exhibits the highest intensities among the four samples, show-

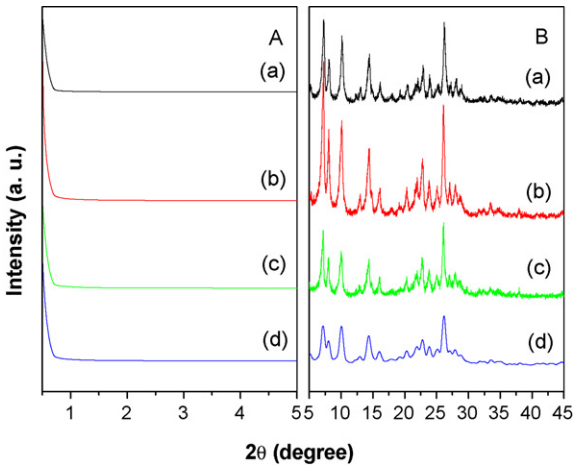

Fig. 1. XRD patterns of MCM-22 with Si/Al molar ratio of 15 (a), 25 (b), 35 (c), and 45 (d).

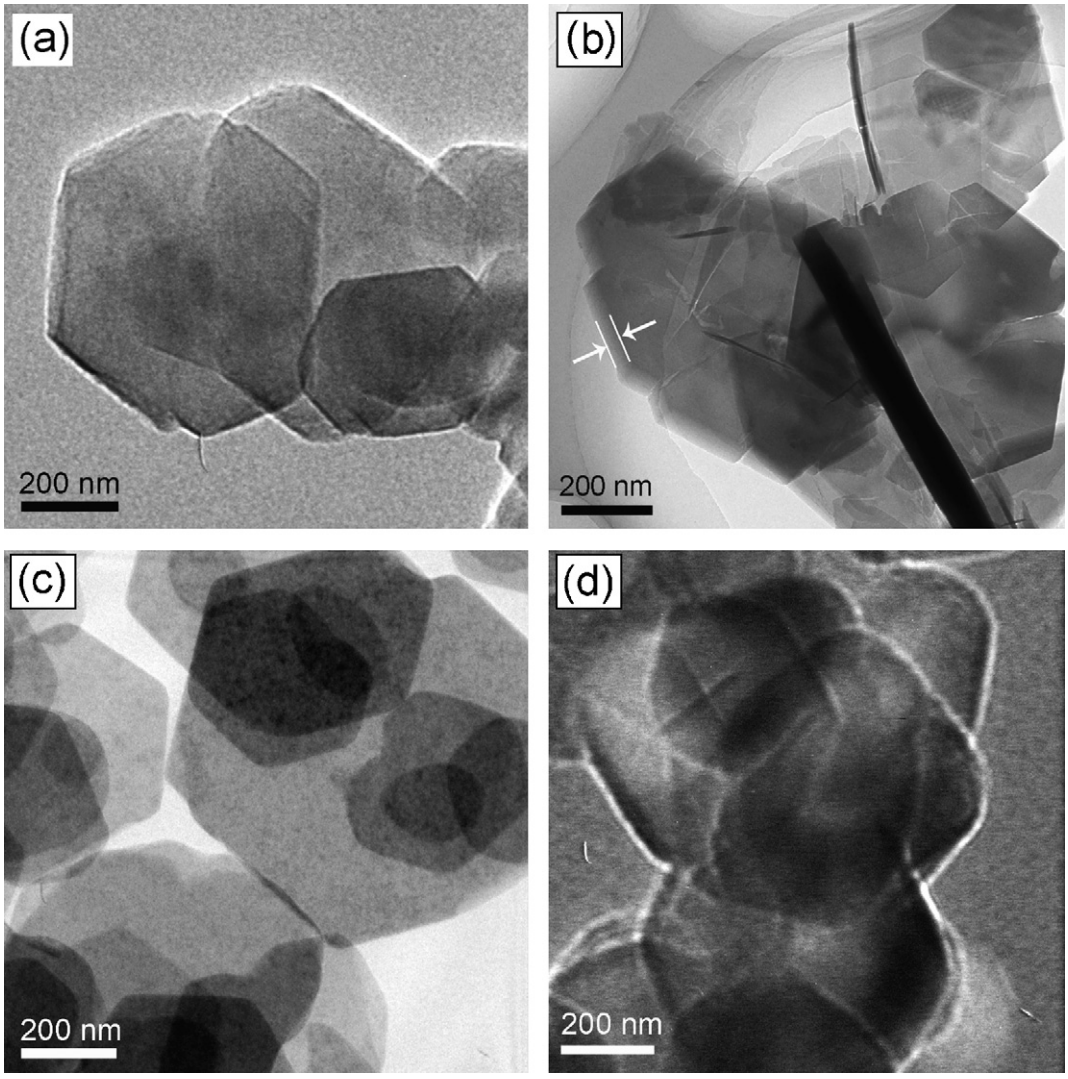

Fig. 2. TEM images of MCM-22 with Si/Al molar ratio of 15 (a), 25 (b), 35 (c), and 45 (d).

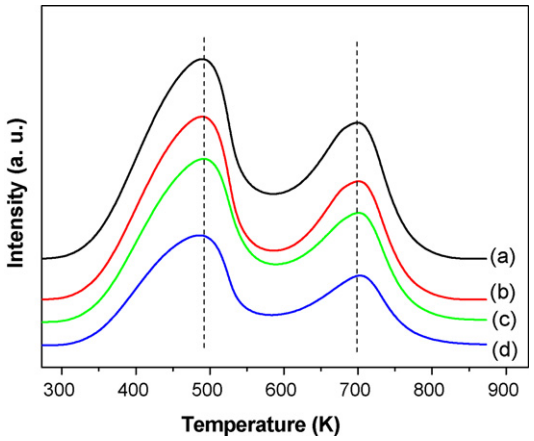

Fig. 3. NH_3-TPD profiles of MCM-22 with Si/Al molar ratio of 15 (a), 25 (b), 35 (c), and 45 (d).

ing the highest crystallinity of the sample. When the Si/Al ratio is increased to 45, the intensities of the XRD patterns show an obvious reduction in comparison with those for HMCM-22 with Si/Al = 25. The results are in good agreement with the facts reported by the literature [27].

Fig. 2 displays the representative TEM images of MCM-22 zeolites with different Si/Al ratios, respectively. It can be observed that the morphologies of all the samples are hexagonal lamellar crystals with the size of about 500–600 nm in diameter and less than 50 nm in thickness. It should be noted that the features of the as-synthesized MCM-22 zeolites are markedly differed from those synthesized in the literatures [22,28], where the crystals of MCM-22 were plates/discs of approximate 1–2 μm in diameter and 0.2–0.3 μm in thickness, usually bunching into 4–8 μm aggregation. Furthermore, it can be also found that the morphology of MCM-22 with Si/Al = 45 shows some difference from other samples, exhibiting less uniform shape and some distant aggregation.

The NH_3-TPD profiles of MCM-22 zeolites with different Si/Al ratios are presented in Fig. 3. It can be seen that the ammonia desorption spectra of all the samples exhibit the typical double-peak characteristic of zeolites with MFI structure

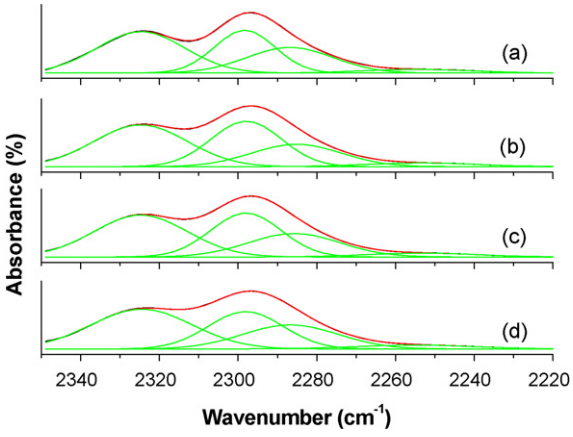

Fig. 4. FT-IR spectra after adsorption of d_3-acetonitrile of MCM-22 with Si/Al molar ratio of 15 (a), 25 (b), 35 (c), and 45 (d).

Table 1
Concentration of the Brønsted and Lewis acid sites of MCM-22 different Si/Al molar ratio

Samples	Concentration of Brønsted acid sites (mmol/g)	Concentration of Lewis acid sites (mmol/g)
MCM-22-15	0.285	0.168
MCM-22-25	0.401	0.171
MCM-22-35	0.298	0.159
MCM-22-45	0.194	0.151

[29,30]. The strong peak at 490 K can be associated with the desorption of physisorbed ammonia and/or ammonia adsorbed on weak acid sites, and the strong peak at about 700 K may be attributed to the desorption of ammonia adsorbed on strong acid sites. The TPD results also suggest that the intensities of both strong acid sites and weak acid sites decrease with increasing Si/Al ratios.

Fig. 4 represents the IR spectra of the C≡N vibrations of d_3-acetonitrile adsorption of MCM-22 with different Si/Al ratios, and the corresponding calculated concentration of acid sites are summarized in Table 1. As shown in the figure, the IR spectra are deconvoluted into four typical bands. The two typical bands at 2296 and 2323 cm^{-1} with high intensity can be assigned to the d_3-acetonitrile adsorption on strong Brønsted acid sites (Si–OH–Al groups) and Lewis acid sites (Al–Lewis sites), respectively. And the other two bands with low intensity centered at 2280 and 2253 cm^{-1} reflect the weak coordination of the C≡N groups to terminal Si–OH groups and C–^{2}H vibrations [23,31]. In Table 2, the calculated concentrations of acid sites are 0.285 and 0.401 mmol/g for MCM-22 with Si/Al = 15 and 25, respectively. While the concentration of Lewis acid sites changes slightly. When the Si/Al ratio is increased from 25 to 45, the concentration of Brønsted acid sites markedly decrease from 0.401 to 0.194 mmol/g. It is well known that the amount of Al in the framework of zeolites usually corresponds to the concentration of Brønsted acid sites. So it can be deduced that not all the Al atoms are incorporated the framework of MCM-22 zeolites during the synthesis process for MCM-22 with Si/Al = 15. The results are consistent with the literature [32].

Because of the highest crystallinity and concentration of acid sites for MCM-22 with Si/Al = 25, it was used to prepare Pd/MCM-22 catalyst to examine the catalytic behavior in one-step synthesis of MIBK in the following process.

Table 2
Textural parameters of pure MCM-22 and Pd/MCM-22 catalysts with different amount of Pd loading

Samples	S_{BET} (m^2/g)	$S_{mesopore}$ (m^2/g)	V_{total} (cm^3/g)	D (nm)
MCM-22	669	89	0.38	4.58
0.2%Pd/MCM-22	628	80	0.36	4.33
0.5%Pd/MCM-22	611	61	0.35	4.21
1.0% Pd/MCM-22	545	49	0.33	4.02

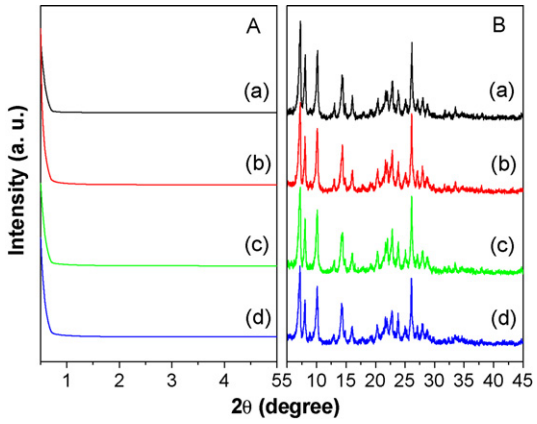

Fig. 5. XRD patterns of parent MCM-22 (a) and Pd/MCM-22 catalysts with Pd loading of 0.2% (b), 0.5% (c), and 1.0% (d).

3.2. Characterization of the Pd/MCM-22 catalysts with different amount of Pd loading

XRD patterns of parent MCM-22 and Pd/MCM-22 catalysts with different amount of Pd loading are shown in Fig. 5. The typical characteristic diffractions of MCM-22 are observed except for a slight decrease of the intensities with increasing Pd loading. The results indicate that introduction of Pd particles into MCM-22 zeolite has not changed the crystal structure of MCM-22 zeolite. Furthermore, no characteristic diffractions of crystalline PdO_x can be detected in the spectra, implying the uniform distribution of the particles throughout the matrix of zeolite or in an amorphous phase.

SEM images of parent MCM-22 zeolite and Pd/MCM-22 catalysts with different amount of Pd loading are displayed in Fig. 6. It can be seen that parent MCM-22 zeolite consist of uniform disk-like platelets with a diameter of about 0.5 μm and a thickness of about 50 nm. As for the Pd/MCM-22 catalysts, the morphologies of the samples change slightly, except for some distant aggregation of the thin disk-like particles, which may be caused by the heat treatment.

The representative TEM images of parent MCM-22 and 0.5%Pd/MCM-22 catalyst are given in Fig. 7. It can be seen that the features of the Pd-loaded sample change slightly, demonstrating the conservation of the morphology after the deposition of Pd particles onto the surface of MCM-22 zeolite.

The N_2 adsorption/desorption analysis is a useful tool to examine the textural characteristics of the porous materials. The isotherms of parent MCM-22 and Pd-loaded samples are depicted in Fig. 8, and the corresponding pore size distributions are displayed in Fig. 9 as well. As shown in Fig. 8, all the isotherms of the samples are similar with a hysteresis loop at high relative pressure (p/p_0), indicating that the crystal sizes are small and presenting a relatively high external surface area with little mesoporosity [33]. Therefore, it can be deduced that the deposition of Pd particles onto the surface of MCM-22 zeolite has little influence on the porous structure of parent MCM-22 zeolite, which are well consistent with above XRD and TEM results. It can be also seen from the figure that the hysteresis loops become

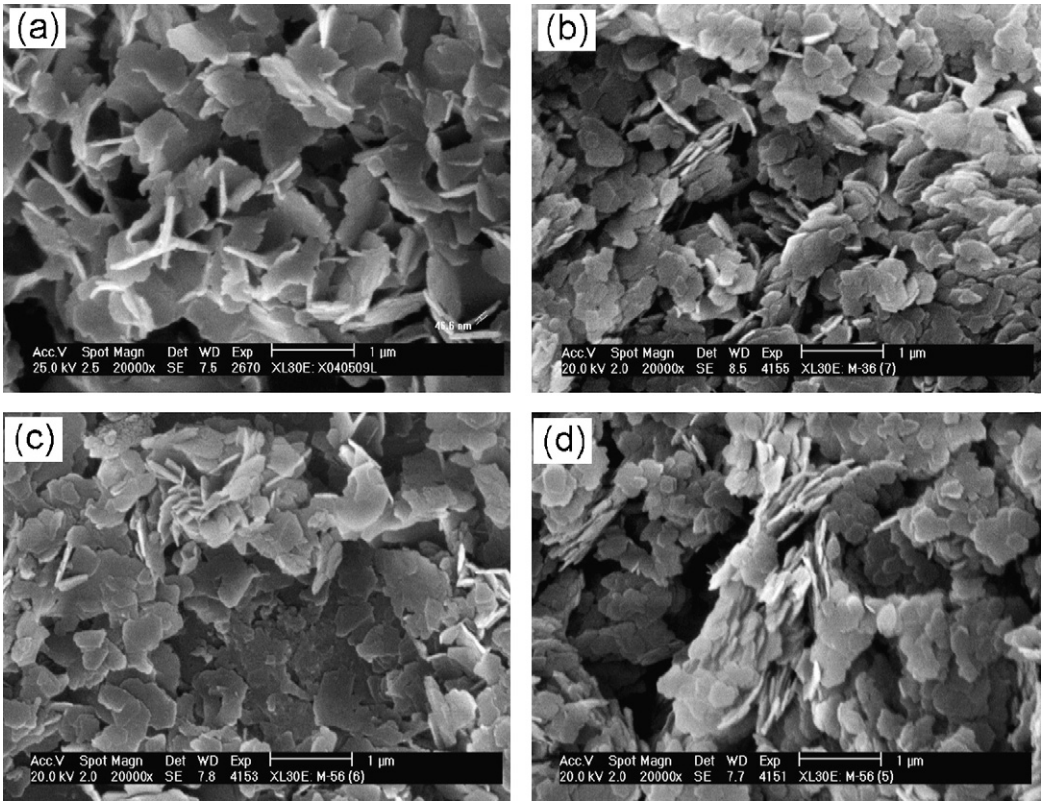

Fig. 6. SEM images of parent MCM-22 (a) and Pd/MCM-22 catalysts with Pd loading of 0.2% (b), 0.5% (c), and 1.0% (d).

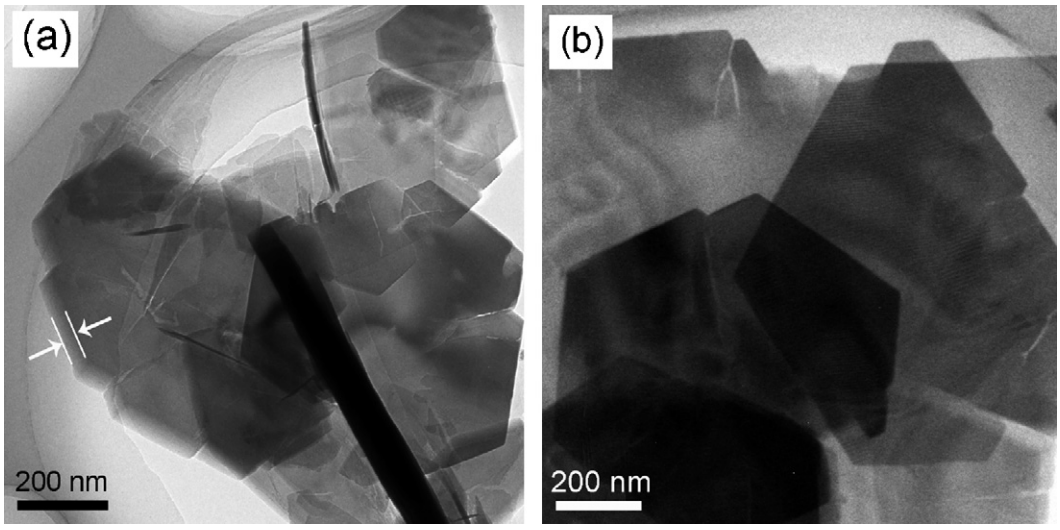

Fig. 7. TEM images of parent MCM-22 (a) and 0.5%Pd/MCM-22 (b).

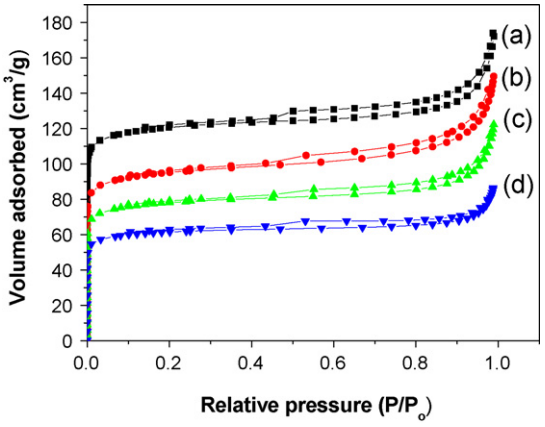

Fig. 8. N_2 adsorption/desorption isotherms of pure MCM-22 (a) and Pd/MCM-22 catalysts with Pd loading of 0.2% (b), 0.5% (c), and 1.0% (d).

smooth in comparison with that of pure MCM-22. As expected, the pore sizes of the samples (Fig. 9) decrease with increasing Pd loading. The textural parameters of the corresponding materials are summarized in Table 2. As shown in the table, the parent MCM-22 has high BET surface area (669 m^2/g), pore volume (0.38 cm^3/g), and average diameter (4.58 nm), which can be attributed to the large supercages in MCM-22 zeolite [34]. For the Pd-loaded samples, high specific surface area can be still obtained, demonstrating its potential application in catalytic reactions. Furthermore, the specific surface area, pore volume, and average pore diameter all decrease with increasing Pd loading, which may be caused by the covering of Pd particles onto the surface of zeolite or partial pore blocking of the channels by the large size particles for high Pd loading.

As shown in the NH_3-TPD profiles (Fig. 10) of Pd/MCM-22 catalysts with different amount of Pd loading, the location and intensity of the peak at low temperature change slightly, whereas the peak at high temperature shifts to lower temperature and the intensities decrease with Pd loading in comparison with that of parent MCM-22. The results indicates that introduction of metal Pd mainly reduces the strong acid sites.

Table 3 lists the concentration of the acid sites of the Pd/MCM-22 catalysts with different amount of Pd loading. It can be seen that the calculated concentrations of Brønsted acid sites decreased from 0.401 to 0.253 mmol/g with the increasing

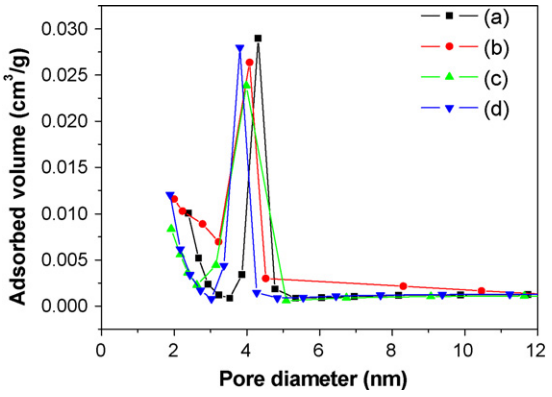

Fig. 9. Pore size distributions for parent MCM-22 (a) and Pd/MCM-22 catalysts with Pd loading of 0.2% (b), 0.5% (c), and 1.0% (d).

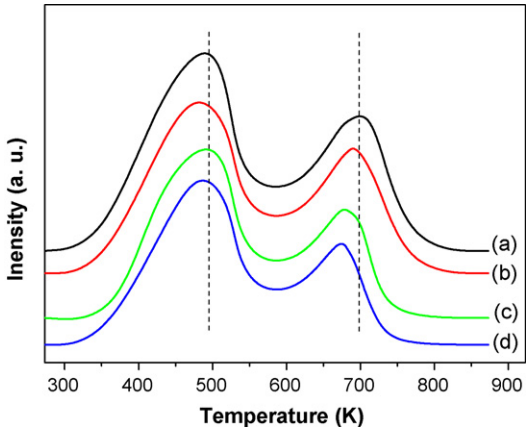

Fig. 10. NH_3-TPD profiles of parent MCM-22 (a) and Pd/MCM-22 catalysts with Pd loading of 0.2% (b), 0.5% (c), and 1.0% (d).

Table 3
Concentration of the Brønsted and Lewis acid sites of pure MCM-22 and Pd/MCM-22 catalysts with different amount of Pd loading

Samples	Concentration of Brønsted acid sites (mmol/g)	Concentration of Lewis acid sites (mmol/g)
HMCM-22	0.401	0.171
0.2%Pd/MCM-22	0.362	0.167
0.5%Pd/MCM-22	0.302	0.165
1.0%Pd/MCM-22	0.253	0.156

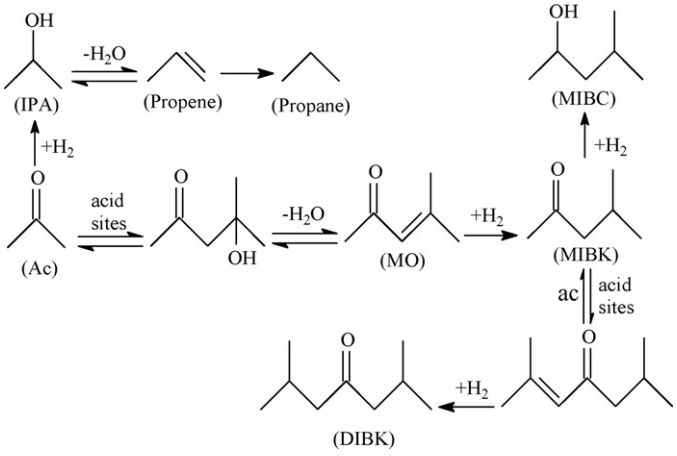

Scheme 1. Main reactions during acetone transformation reaction.

Pd loading from 0 to 1.0%, while the concentration of Lewis acid sites decreases slightly. The decrease of the concentration of the acid sites may be attributed to the covering of the acid sites on the surface by the metal Pd particles.

H_2-TPD data of the Pd/MCM-22 catalysts with different amount of Pd loading are list in Table 4. As revealed in the table, the amount of Pd dispersion decreases from 79.5 to 28.2% and Pd average particle size increase from 1.08 to 3.61 nm with increasing Pd loading from 0.2 to 1.0. The results indicate that the increase of Pd loading dramatically decreases the Pd dispersion and enlarges the particle size.

3.3. Catalytic results

The products resulting from acetone (Ac) transformation are propene and propane (Pc), isopropyl alcohol (IPA), methyl isobutyl ketone (MIBK), methyl isobutyl carbinol (MIBC), diisobutyl ketone (DIBK) and its isomer, respectively. Formation of the products can be explained as Scheme 1 [17,35]. Diacetone alcohol formed by the aldol condensation of acetone on acid sites is dehydrated to mesityl oxide, which is hydrogenated to methyl isobutyl ketone on metallic sites. MIBK may go through additional condensation and hydrogenation steps to form diisobutyl ketone, or it may be hydrogenated to form methyl isobutyl carbinol. Along a parallel reaction, acetone can also be directly hydrogenated to isopropanol (IPA), which is dehydrated to propene and further hydrogenated to propane.

3.3.1. Effect of amount of Pd loading

Influence of Pd loading on the catalytic performance in one-step synthesis of MIBK is given in Table 5. As shown in the table, the acetone conversion increases and the selectivity for MIBK decreases with increasing Pd loading. Furthermore, the selectivity for Pc and IPA (associated with hydrogenation) increases, while the selectivity for DIBK (further condensation product) decreases with Pd loading. The results indicate that Pd/MCM-22 catalyst with high Pd loading favor the hydrogenation of C=O of acetone to IPA in the competition between the hydrogenation and the condensation. This can be explained by the increased particle size for the catalyst with high Pd loading. As revealed from the H_2-TPD results (Table 4), the large particle size caused by the aggregation of metal particles may result in the fewer possibilities of Pd particles entering the channel of the zeolites. Therefore, most of the Pd particles are deposited on the external surface, while the acidic sites which are necessary for the condensation are mainly in the channels [34]. As a result, the direct hydrogenation to IPA from acetone is favored and the condensation is suppressed. Moreover, the covering of surface of the zeolites by the Pd particles may also results in the reduction of the acid sites. As shown in Fig. 10 and Table 3, the total acidity and the concentration of acid sites of Pd/MCM-22 all markedly decrease with Pd loading. On basis of above analysis, it can be deduced that the large particle size and the reduction of acidity may be the main reasons for the decrease of the selectivity for MIBK and the increase of IPA. Because the formation of MIBK needs the cooperation between metallic and acidic sites, while hydrogenation of acetone to IPA only needs metallic sites [35].

3.3.2. Effect of H_2/acetone molar ratio

Influence of H_2/acetone molar ratios on MIBK synthesis is shown in Table 6. It can be seen that the acetone conversion increases with an increase of H_2/acetone ratio, while the selectivity for MIBK decreases. Moreover, the selectivities for the products related with hydrogenation reaction, such as IPA and Pc, increase greatly with increasing H_2/acetone ratio. And the formation of DIBK is affected slightly.

Table 4
H_2-TPD data of Pd/MCM-22 catalysts with different amount of Pd loading

Samples	Pd loading (wt %)	Metal sites (μmol/g-cat)	Pd dispersion (%)	Average particle size (nm)
0.2%Pd/MCM-22	0.17	1.6	79.5	1.08
0.5%Pd/MCM-22	0.48	4.1	59.4	1.52
1.0%Pd/MCM-22	0.95	8.1	28.2	3.61

Table 5
Effect of amount of Pd loading on the catalytic performance in one-step synthesis of MIBK over Pd/MCM-22 catalysts (reaction conditions: $T = 433$ K, $P = 40$ atm, and H_2/acetone = 0.2)

Conversion and selectivity	Amount of Pd loading (wt%)			
	0.1	0.2	0.5	1.0
Conversion (%)	26.4	29.7	34.0	35.2
Selectivity (%)				
MIBK	87.9	87.3	86.9	69.2
Pc	1.2	2.8	4.3	6.7
IPA	0.9	1.4	2.5	16.8
DIBK	6.5	5.5	4.1	3.2
MIBC	0.8	1.1	1.3	1.9
Unknown[a]	1.3	1.9	0.9	2.2

[a] Not detectable by GC, estimated from the lack of the C balance (conversion –Σ products analyzed by GC).

Table 6
Effect of H_2/acetone molar ratio on the catalytic performance in one-step synthesis of MIBK over Pd/MCM-22 (reaction conditions: $T = 433$ K, $P = 40$ atm, and Pd loading = 0.5%)

Conversion and selectivity	H_2/acetone molar ratio				
	1	0.5	0.33	0.25	0.2
Conversion (%)	38	36.9	35.2	34.8	34.0
Selectivity (%)					
MIBK	69.6	74.1	80.2	83.4	86.9
Pc	11.3	9.3	6.2	4.1	4.3
IPA	12.7	10.2	7.1	5.2	2.5
DIBK	4.1	4.3	3.5	4.4	4.1
MIBC	0.9	1.1	1.3	1.1	1.3
Unknown[a]	1.3	1.9	1.8	1.8	0.9

[a] As in Table 5.

3.3.3. Effect of reaction temperature

Table 7 shows the effect of temperature on MIBK synthesis over 0.5% Pd/MCM-22. The results indicate that the conversion of acetone increases monotonically with reaction temperature. The selectivity for MIBK increases before 433 K, but decreased when the temperature is increased beyond 433 K, which may be attributed to the enhanced formation of over-condensed by-product (DIBK). Furthermore, the selectivity for IPA decreases markedly with the increasing temperature, while the selectivity for Pc increases from 1.3% to 7.8% in the temperature range. These results demonstrate that the direct hydrogenation activity is favored by lower temperature, while condensation and dehydration catalyzed by acid sites are favored by high temperature. The optimum temperature range for the MIBK synthesis is between 413 and 453 K.

Table 7
Effect of reaction temperature on the catalytic performance in one-step synthesis of MIBK over Pd/MCM-22 (reaction conditions: $P = 40$ atm, H_2/acetone = 0.2, and Pd loading = 0.5%)

Conversion and selectivity	Temperature (K)				
	393	413	433	453	473
Conversion (%)	29.6	32.2	34.0	34.6	35.8
Selectivity (%)					
MIBK	82.6	84.4	86.9	81.1	78.0
Pc	1.3	1.6	4.3	6.1	7.8
IPA	11.9	7.8	2.5	2.0	1.6
DIBK	0.9	2.6	4.1	7.9	11.5
MIBC	0.9	1.1	1.3	0.9	0.8
Unknown[a]	2.4	2.5	0.9	2.0	0.3

[a] As in Table 5.

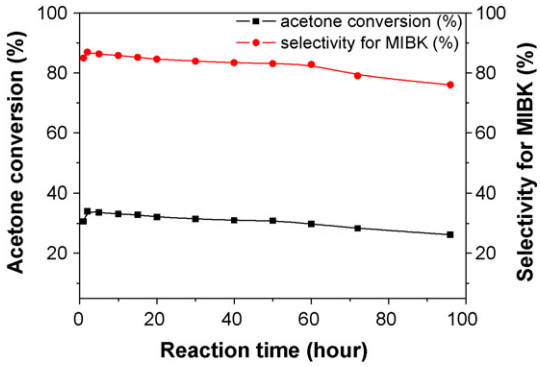

Fig. 11. The stability test for 0.5%Pd/MCM-22 catalyst in one-step synthesis of MIBK as a function of reaction time (reaction conditions: $T = 433$ K, $P = 40$ atm, and H_2/acetone = 0.2).

3.3.4. Stability test

The stability test result for 0.5%Pd/MCM-22 catalyst performing at 433 K, 40 atm and hydrogen/acetone = 0.2 is displayed in Fig. 11. It can be seen that the acetone conversion only declines from 34% to 31.9% and the selectivity for MIBK decrease from 86.9% to 82.8% after 60 h of reaction time. The result demonstrates that the 0.5%Pd/MCM-22 catalyst is an effective and relatively stable catalyst for one-step synthesis of MIBK from acetone in gas phase.

4. Conclusions

In summary, high crystalline and pure MCM-22 was dynamically synthesized by hydrothermal method, showing much smaller crystal than those in the literatures. Pd-supported MCM-22 catalyst showed high catalytic activity in one-step synthesis of MIBK from acetone, and 34% of acetone conversion and 86.9% of selectivity for MIBK were obtained. The particle size and the acidity of the catalysts played an important role to obtain high catalytic activity and selectivity of MIBK. A proper balance between metallic and acidic sites appeared to be necessary to realize high catalytic performance. In addition, the catalyst showed relative high stability, suggesting it's a candidate catalyst in one-step synthesis of MIBK from acetone.

Acknowledgements

Financial supports from the National Natural Science Foundation of China (Grant number 20273025) and the foundation of Harbin Engineering University (Grant number 002100260719) are greatly acknowledged.

References

[1] M.K. Rubin, P. Chu, U.S. Patent 4,954,325 (1990).
[2] M.F. Leonowicz, J.A. Lawton, S.L. Lawtonand, M.K. Rubin, Science 264 (1994) 1910.
[3] J.K. Kushnerick, P. Boothwyn, D.O. Marler, J.P. Mcwilliams, U.S. Patent 4,992,606 (1991).
[4] J. Rigoreau, S. Laforge, N.S. Gnep, M. Guisnet, J. Catal. 236 (2005) 45.
[5] P. Chu, G. W. Kirker, J.D. Kusherick, D.O. Marler, U.S. Patent 5,043,512 (1991).
[6] H.J. Jung, S.S. Park, C.H. Shin, Y.K. Park, S.B. Hong, J. Cata. 245 (2007) 65.
[7] G.W. Kirker, S. Mirzahi, S.S. Shih, U.S. Patent 5,000,839 (1991).
[8] X.X. Zhu, S.L. Liu, Y.Q. Song, S.J. Xie, L.Y. Xu, Appl. Catal. A: Gen. 290 (2005) 191.
[9] W. Reith, M. Dettmet, H. Widdecke, B. Fleischer, Study Surf. Sci. Catal. 59 (1991) 487.
[10] K. Schmitt, J. Distodorf, W. Flakus, U.S. Patent 3,953,517 (1976).
[11] F. Winter, M. Wolters, A. Jos van Dillen, K.P. de Jong, Appl. Catal. A: Gen. 307 (2006) 231.
[12] L.M. Gandia, M. Montes, Appl. Catal. A: Gen. 101 (1993) L1.
[13] Y. Higashio, T. Nakayama, Catal. Today 28 (1996) 127.
[14] L. Melo, G. Giannetto, F. Alvarez, P. Magnoux, M. Guisnet, J. Mol. Catal. A: Gen. 124 (1997) 155.
[15] V. Chikan, A. Molnar, K. Balazsk, J. Catal. 184 (1999) 134.
[16] L.M. Gandia, R. Malm, R. Marchand, R. Conanec, Y.L. Laurent, Appl. Catal. A: Gen. 114 (1994) L1.
[17] K.H. Lin, A.N. Ko, Appl. Catal. A: Gen. 147 (1996) L259.
[18] P.Y. Chen, S.J. Chu, C.C. Chen, N.S. Chang, W.C. Lin, T.K. Chuang, U.S. Patent 5,059,724 (1991).
[19] S. Narayanan, R. Unnikrishnan, Appl. Catal. A: Gen. 145 (1996) 231.
[20] P.P. Yang, J.F. Yu, Z.L. Wang, M.P. Xu, Q.S. Liu, X.W. Yang, T.H. Wu, Catal. Commun. 6 (2005) 107.
[21] Y.Z. Chen, B.J. Liaw, H.R. Tan, K.L. Shen, Appl. Catal. A. Gen. 205 (2001) 61.
[22] A. Corma, C. Corell, J. Pérez-Pariente, Zeolites 15 (1995) 2.
[23] B. Wichterlová, Z. Tvarůžková, Z. Sobalik, P. Sarv, Micropor. Mesopor. Mater. 24 (1998) 223.
[24] J. Čejka, A. Krejčí, N. Žiková, J. Kortrla, S. Ernst, A. Weber, Micropo. Mesopo. Mater. 53 (2002) 121.
[25] J.A. Amelse, L.M. Schwartz, J.B. Butt, J. Catal. 72 (1981) 95.
[26] E.L. Rodrigues, J.M.C. Bueno, Appl. Catal. A: Gen. 232 (2002) 147.
[27] I. Mochida, S. Eguchi, M. Hironaka, S. Nagao, K. Sakanishi, D.D. Whitehurst, Zeolites 142 (1997) 18.
[28] G.G. Juttu, R.F. Lobo, Micropor. Mesopor. Mater. 40 (2000) 9.
[29] J.G. Post, J.H.C. van Hoff, Zeolites 4 (1984) 9.
[30] P. Wu, Q.B. Kan, X.X. Wang, D.Y. Wang, H.J. Xing, P.P. Yang, T.H. Wu, Appl. Catal. A: Gen. 282 (2005) 39.
[31] A.G. Pelmenschikov, R.A. van Santen, J. Jänchen, E. Meijer, J. Phys. Chem. 97 (1993) 11071.
[32] K. Okumura, M. Hashimoto, T. Mimura, M.K. Niwa, J. Catal. 206 (2002) 23.
[33] A. Corma, U. Diaz, V. Fornés, J.M. Guil, J. Martínez-Triguero, E.J. Ceyghtony, J. Catal. 191 (2000) 218.
[34] N. Kumar, R. Byggningsbacka, M. Korpi, L. Linfors, T. Salmi, Appl. Catal. A: Gen. 227 (2002) 97.
[35] S.M. Yang, Y.M. Wu, Appl. Catal. A: Gen. 192 (2000) 211.